nature communications

Article

https://doi.org/10.1038/s41467-024-53543-4

Investigating proton shuttling and electrochemical mechanisms of amines in integrated CO_2 capture and utilization

Received: 5 December 2023

Accepted: 8 October 2024

Published online: 24 October 2024

Check for updates

D. F. Bruggeman, G. Rothenberg & A. C. Garcia

Carbon capture and utilization (CCU) technologies present a promising solution for converting CO_2 emissions into valuable products. Here we show how amines, such as monoethanolamine (MEA) and 2-amino-2-methyl-1-propanol (AMP), influence the electrochemical CO_2 reduction process in an integrated CCU system. Using in situ spectroscopic techniques, we identify the key roles of carbamate bond strength, proton shuttling, and amine structure in dictating reaction pathways on copper (Cu) and lead (Pb) electrodes. Our findings demonstrate that on Cu electrodes, surface blockage by ammonium species impedes CO_2 reduction, whereas on Pb electrodes, proton shuttling enhances the production of hydrocarbon products. This study provides additional insights into optimizing CCU systems by tailoring the choice of amines and electrode materials, advancing the selective conversion of CO_2 into valuable chemicals.

Carbon Capture and Utilization (CCU) technologies are a viable strategy for bridging fossil-generated CO_2 and useful carbon building blocks and thus mitigating the increase in the concentrations of CO_2 present in the atmosphere[1]. Amine-based solvents have been intensively studied in integrated electrochemical CO_2 capture and conversion systems due to their moderate interaction with carbon dioxide molecule (CO_2)[2–4]. CO_2 can be chemisorbed on amines (amine−CO_2) via a nucleophilic reaction to yield the corresponding carbamates (R−COO^-) and ammonium species (R−H^+) (Fig. 1A)[5]. Amines are interesting because their molecular structure can be altered, allowing a fine-tuning of their CO_2-capturing abilities[6].

CCU processes comprise three important steps: CO_2 separation from the gas mixture, its release and capture material regeneration, and electrochemical conversion (Fig. 1B). Electrochemical methods are gaining favor over traditional temperature or pressure modulation for their energy efficiency[7,8]. These methods usually function as separate units, providing flexibility but requiring multiple systems.

Recent studies indicate that integrating the capture and conversion processes may improve energy efficiency and potentially reduce costs (Fig. 1C, D). For example, using captured CO_2 directly in electrolysis circumvents the energy-intensive desorption step, leading to cost savings on CO_2 compression and equipment. Energy analyses indicate potential energy savings of up to 44% for integrated systems over traditional ones[9].

The integration processes, however, introduce complex physicochemical and engineering considerations, necessitating a reevaluation of existing knowledge and exploration of new scientific frontiers. One key aspect of this integrated approach is the pH-dependent behavior of CO_2 capture using aqueous amines, which notably influences both the capture efficiency and the subsequent electrochemical conversion process.

For instance, studies by Morales-Guio et al.[10], and Gallant et al.[11] delved into the pH dependence on the interaction between amines and CO_2, which leads to the formation of species like carbamates and bicarbonates, whose equilibrium is highly sensitive to the solution pH. The pH can influence the competitive adsorption of different species at the electrode interface, affecting electron transfer to the desired carbamate active species and ultimately the efficiency of CO_2 reduction. Their results suggest that the molecular design of amines, including their pKa, provides a means to tailor the capture-conversion process by affecting the initial reaction rate with CO_2, the strength of bonding with CO_2, and the pH of the solution. Amines with different pKa values can be used to optimize the capture solution pH to balance

Van't Hoff Institute for Molecular Sciences, University of Amsterdam, Science Park 904, Amsterdam, The Netherlands. e-mail: a.c.garcia@uva.nl

https://doi.org/10.1038/s41467-024-53543-4

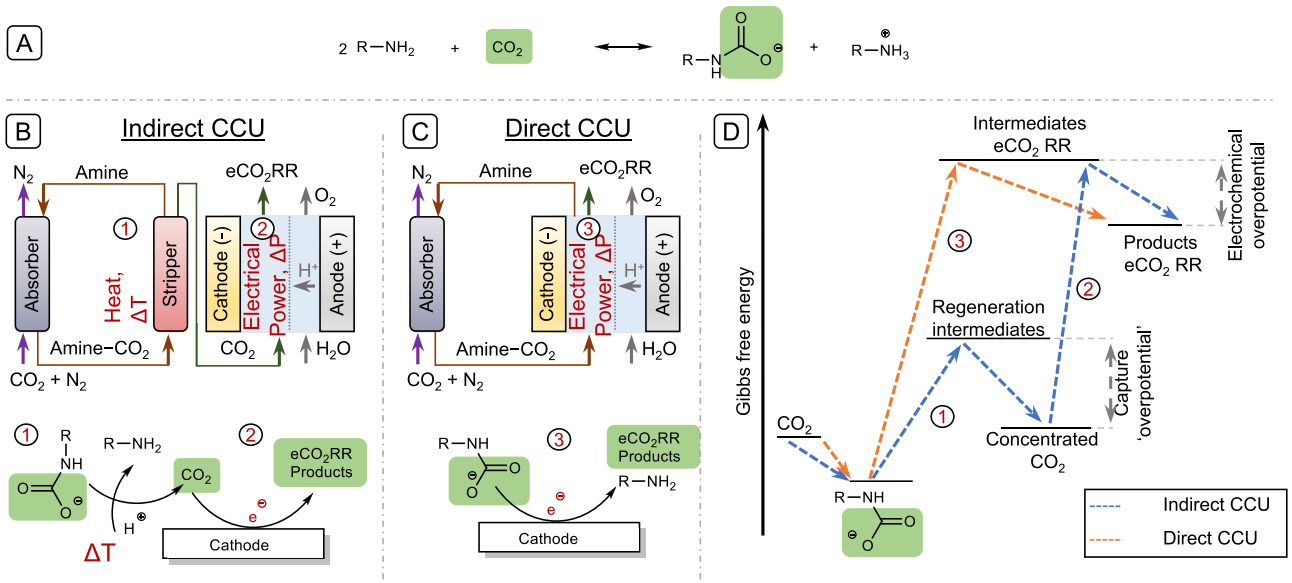

Fig. 1 | Schematic representation of the integrated CCU (carbon capture and utilization) process. A Carbamate formation of amines and CO_2 via a nucleophilic attack. Schematic overview of electroreduction of CO_2 via **B** indirect or **C** direct carbamate reduction and **D** CO_2 capture and conversion energetics for indirect and direct CCU (adapted from ref. 18). CCU Carbon capture and utilization, eCO_2RR electrochemical reduction reaction of CO_2.

the demands for efficient CO_2 capture and favorable conditions for electrochemical conversion.

A significant pH drop during capture can also promote the hydrolysis of the carbamate to bicarbonate, complicating the determination of carbamate involvement in aqueous conditions[12]. Depending on the electrolyte medium, electrochemically reactive capture can produce a variety of products frequently with high selectivity[12], including CO[7,11,13–15], formic acid[7,13,16], and solid alkali carbonates[17].

These findings are vital for refining integrated CCU systems and enhancing their efficiency and selectivity for various products such as CO, formic acid, and alkali carbonates[12,18–22].

The application of carbamates for direct electrochemical CO_2 reduction is an area of increasing interest. The influence of critical parameters, such as amine type, solvent system, and electrocatalyst selection, along with rate-limiting factors like reactant concentration and reactor conditions, is not understood. This hampers the systematic design of optimized direct capture-electrolysis reactors[12,18,19,21].

For example, due to the multi-ionic nature of amine-based electrolytes, ammonium cations can compete with carbamate species for adsorption sites at the electrode interface, thereby hindering electron transfer to the carbamate[11,23,24]. Thus, the carbamate structure is important, as sterically hindered amines may hamper the surface interactions with the cathode. Once the carbamates are adsorbed at the electrode interface, the ability to facilitate N–C bond breakage will be governed by the amine as well as by the electronic structure of the electrode surface itself. However, the relation of both amine steric/structure and electrode surface is largely unexplored.

Addressing this problem, we study here the combined mechanism of the CO_2-captured amine reduction reaction. We do this by incorporating factors that may affect this process, such as interaction with various electrocatalysts and amine properties, such as steric hindrance, carbamate bond strength, and capacity to increase local proton concentration via the ammonium species.

We designed the experimental setting such that the materials under investigation are substantially different, to maximize the amount of data generated. We prepared amine–CO_2 adducts as the sole CO_2 donor in the electrolyte solution using model amines (Fig. 2A)[25], specifically monoethanolamine (MEA; no steric hindrance,

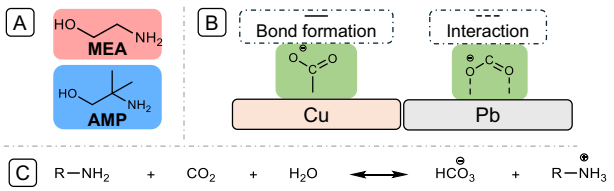

Fig. 2 | Interaction of amine on the electrode surface. A The used amines in this study and **B** the visualization of inner-sphere (Cu) and outer-sphere (Pb) electron transfer mechanisms. **C** The schematic overview of the bicarbonate production (HCO_3^-) in the presence of amines and CO_2. MEA monoethanolamine, AMP 2-amino-2-methyl-1-propanol.

strong CO_2 bond)[26] and 2-amino-2-methyl-1-propanol (AMP; sterically hindered, weak CO_2 bond)[27]. These were tested with two solid electrocatalysts (Fig. 2B)[28]: Cu (inner-sphere electrode, i.e., electron transfer with chemical-bond formation or rearrangement at the electrode surface)[29,30] and Pb (outer-sphere electrode, i.e., the electrons transfer by tunneling between the electrode and the substrate through a solvent layer)[31].

The organic solvent sulfolane[12] was used to solubilize amine and carbamate/ammonium ($R–COO^-/–H^+$) species, thus preventing the formation of insoluble carbonate ions (CO_2^{2-}) and bicarbonate, which are promoted by the presence of water[12]. This approach avoids the complexities introduced by water acting as a proton shuttle and allows us to focus on the role of carbamate species as the sole CO_2 donor.

By combining cyclic voltammetry (CV), in situ Fourier Transform Infra-Red (FTIR) spectroscopy, and bulk electrolysis, we could pinpoint the distinct behaviors exhibited by amine–CO_2 adducts in comparison to dissolved CO_2. On the Cu electrode, the ammonium species formed during the CO_2 collection step take precedence over the CO_2 reduction process. We hypothesized that MEA–H^+ prevents surface interaction with released CO_2, whereas AMP–H^+ allows for some CO_2 reduction thanks to steric hindrance. Conversely, Pb electrode lacks surface interactions, leading to a more dynamic surface environment.

The presence of extra protons from ammonium species promotes the production of protonated products of electrochemical CO_2 reduction reaction (eCO_2RR). Comparing MEA and AMP, MEA–H^+

shows stronger proton shuttling capabilities, resulting in higher proton content in C_2 products. This suggests that MEA–H^+ is less constrained by steric hindrance. This study highlights the crucial role of the cathode when paired with the CO_2 capture agent and expands fundamental knowledge on the functioning of a fully integrated CCU system.

Results and discussion

Cyclic voltammetry

We studied the differences in kinetics between freely dissolved and bounded (to our two model amines—MEA and AMP) CO_2 using cyclic voltammetry (CV). In a typical experiment, CO_2 is captured by the amines by saturating the electrolyte containing 1.0 M of the amine with CO_2. Then, the solution is purged with N_2 to eliminate all the dissolved CO_2 (Fig. S2) This process yields the amine–CO_2 adducts of MEA or AMP (MEA–CO_2 or AMP–CO_2, respectively) consisting of ammonium (MEA–H^+ or AMP–H^+, respectively) and a carbamate (MEA–COO^- or AMP–COO^-, respectively) species. As a result, the carbamate is the eCO_2RR's sole carbon source.

We chose Cu as working electrode due to its good molecule adsorption properties, primarily driven by its strong affinity for C and H atoms[30]. This choice is driven by our hypothesis that Cu would enhance interactions with carbamates, leading to improved electron transfer. Figure 3A compares the CV profiles for free CO_2, MEA, AMP, and the two CO_2-bound amines MEA–CO_2 and AMP–CO_2.

The CO_2 saturated solution (green line) shows a small increase in current density at −1.57 V vs. Ag/AgCl for eCO_2RR[32]. The lack of reductive waves in the experiments with the free amines (dashed red and blue curves for MEA and AMP, respectively) indicate their electrochemical stability within the potential window. On the Cu electrode, the CV profiles reveal that the amines' ability to capture CO_2 has a considerable impact on their reduction potential, unlike the free amines. While free CO_2 only shows modest activity, MEA–CO_2 and AMP–CO_2 both show a large increase in current density at a lower potential at −1.35 and −1.51 V vs. Ag/AgCl (solid red and blue curves, respectively). The enhanced activity indicates either a different mechanism of the eCO_2RR via the carbamates or the presence of a different reduction reaction. MEA–CO_2 reduces more easily than AMP–CO_2, showing that one of the two species of the MEA–CO_2 couple ($R–COO^-/–H^+$) has a higher affinity to the Cu surface. This implies that, in the case of MEA–CO_2, the reduced steric hindrance increases the amount of substrate available at the surface, and that surface interaction has a greater role.

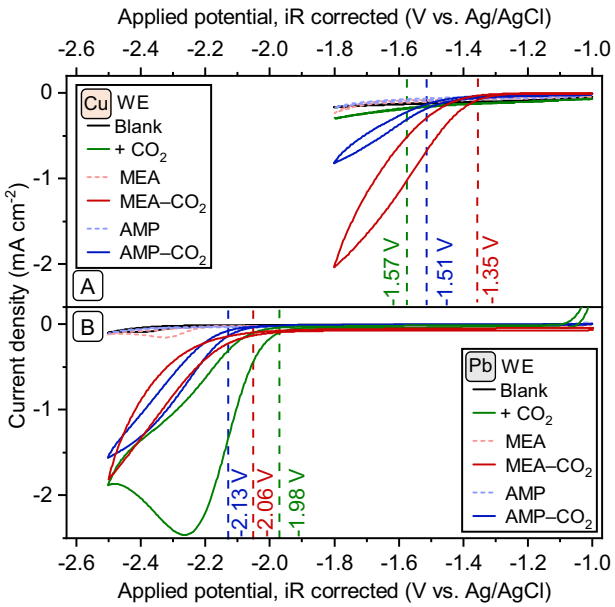

Fig. 3 | Comparison between electrode surface and amine-type structure. Cyclic voltammograms (CVs) of dissolved CO_2, CO_2 captured amines MEA–CO_2 and AMP–CO_2 and the free amines MEA and AMP in sat. TEACl in Sulfolane using a **A** Cu electrode (area = 0.196 cm^2) or **B** Pb electrode (area = 0.196 cm^2) and a RE= Ag/AgCl, CE = Pt, scanning from positive to negative and back at 10 mV s^{-1}, 2nd scan at room temperature. An *i*R compensation of 85% was automatically applied by the potentiostat, CVs without iR compensation are shown in Fig. S18. Average resistance (N = 8) 667±263 Ω and 530±197 Ω for Pb and Cu, respectively. MEA monoethanolamine, AMP 2-amino-2-methyl-1-propanol, vs. versus. Source data are provided as a Source Data file.

Conversely, on the Pb electrode (Fig. 3B), which is more inert due to weaker binding of C and H atoms[33], the free CO_2 reduction takes place at −1.98 vs. Ag/AgCl. A pronounced peak at −2.25 V vs. Ag/AgCl aligns with the diffusion-limited behavior of CO_2, in agreement with previous studies[34]. This confirms that Pb surface follows the outer-sphere electron transfer pathway instead of surface substrate absorption.

Our findings also show that CO_2 adduction by the amines has a significant impact on the applied potential required to initiate a reduction reaction. While the free amines barely show reductive waves, MEA–CO_2 and AMP–CO_2 show an increase of activity at −2.06 and −2.13 vs. Ag/AgCl, respectively. In contrast to Cu electrode, on the Pb electrode the free eCO_2RR is more active than that of the amine–CO_2 species. Furthermore, MEA–CO_2 and AMP–CO_2 show accelerated current density at similar applied potentials on Pb. This contrasts with Cu electrode, where MEA–CO_2 shows an earlier onset than AMP–CO_2. The Pb electrode is less dependent on the carbamate steric hindrance and C–N bond strength (cf. the similar carbamate reduction potentials and current density).

The variance in onset potentials is attributable to the different potentials of zero charge (PZC), which dictates the adsorption preference for anions when the applied potential is higher than the zero-charge potential, and vice versa for cations. For Cu and Pb, the PZCs are +90 mV and −620 mV vs. NHE, respectively[35]. The higher value for of Cu suggests its enhanced ability to attract cations at less negative potentials compared to Pb. This affects the electrochemical reaction kinetics and dictates the location of the reduction wave on the electrode surface. As a result, cationic species, such as protons and MEA/AMP-H^+, preferentially accumulate at Cu, influencing the electrocatalytic activity and surface processes.

In situ FTIR spectroscopy

To gain further insight into the reaction mechanism at the electrode surface, we ran in situ FTIR spectroscopy during the electrochemical sweep. In this way, we can evaluate the N–C bond strength between amines and electrode surface. Figure 4 shows the results (the inset shows the reference spectra of the electrolyte, amines and amine–CO_2 adducts). The hydrogen stretching region is where amines and the electrolyte molecules that undergo C–H, N–H, and O–H stretching also absorb[36]. These various contributions are hard to separate, and the water peak predominates. As a result, the wavenumber range between 3000 and 4000 cm^{-1} has no useful data[37]. Reference spectra of the electrolyte, amine, amine–CO_2 adducts and proposed products are shown in Fig. S3 and Table S1.

Figure 4A–C shows the spectra for the Cu electrode. A summary of the most significant bands and their changes is given in Tables S2 and S3, along with the full spectra of the experiments conducted with and without CO_2 in Fig. S4. Spectra obtained under free CO_2 in the electrolyte (Fig. 4A) reveals a clear immediate consumption/accumulation of CO_2 as a positive band at 2345 cm^{-1} (O = C = O, asymmetric stretch)[30], and the appearance of two negative bands in the region of carboxylic acids (C = O stretch, at 1675 cm^{-1}) and carboxylates (COO^- asymmetric stretch, at 1607 cm^{-1})[38] from −1.5 V vs. Ag/AgCl, which is likely to be the eCO_2RR product formic acid[39]. When CO_2 is captured in AMP (Fig. 4C), an immediate response is observed but

https://doi.org/10.1038/s41467-024-53543-4

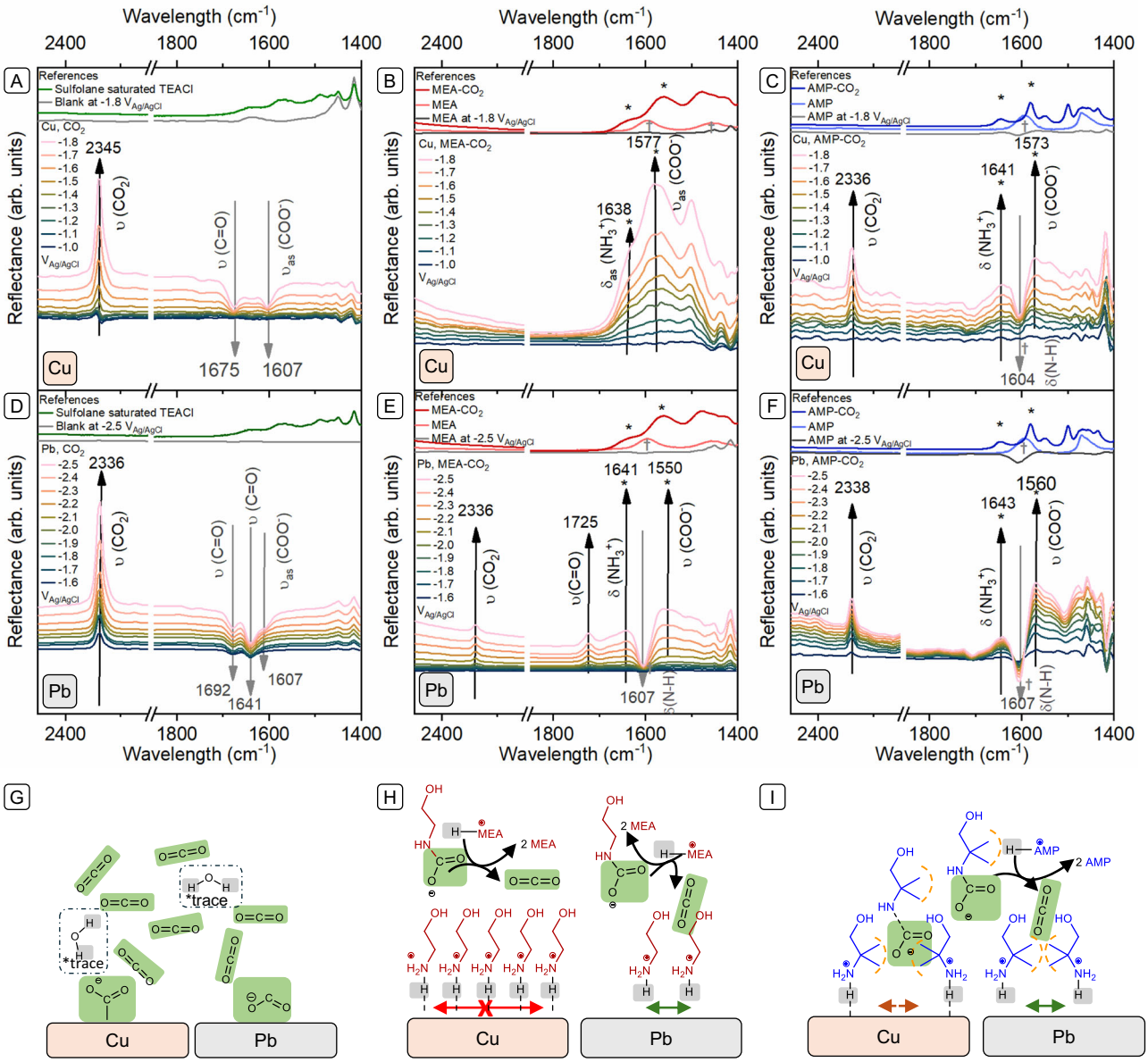

Fig. 4 | Effect of the applied potential on the Amine–CO_2 reduction and its interaction with the electrode surface. In situ FTIR spectra performed during an electrochemical sweep from −1.0 V to −1.8 V vs. Ag/AgCl (from blue to pink) on a Cu electrode with **A** free CO_2, **B** MEA–CO_2, **C** AMP–CO_2, and their reference spectra as inset. In situ FTIR spectra performed during an electrochemical sweep from −1.6 V to −2.5 V vs. Ag/AgCl (from blue to pink) on a Pb electrode with **D** free CO_2, **E** MEA–CO_2, **F** AMP–CO_2, and their reference spectra as inset. The experiment was performed in sat. TEACl in sulfolane at the indicated applied potentials and a reference spectrum was taken at −1.0 V or −1.6 V vs. Ag/AgCl for Cu and Pb, respectively. Schematic view of postulated interactions on the Cu and Pb electrode surface for **G** free CO_2, **H** MEA–CO_2, and **I** AMP–CO_2. MEA= monoethanolamine, AMP = 2-amino-2-methyl-1-propanol. Spectra were collected in duplicate for comparison. Source data are provided as a Source Data file.

show a small increase in intensity after −1.5 V vs. Ag/AgCl in accordance with our cyclic voltammogram results (Fig. 3A). Two positive consumption bands of AMP–CO_2, represented with an ammonium species (NH_3^+, asymmetric bend, at 1641 cm^{-1}) and a carboxylate ((*N*–)COO^-, asymmetric stretch, at 1573 cm^{-1})[37,40], with a combined negative formation band representing an amine (N–H bending, at 1604 cm^{-1})[40] are observed, the latter indicating regeneration of the free amine. A CO_2 consumption band is also visible, with a stronger increase after −1.5 V vs. Ag/AgCl (2336 cm^{-1}). The formation of a band of carboxylic acid (C = O stretch, negative band at 1695 cm^{-1}) is observed, which could pertain to an eCO_2RR product.

Unfortunately, due to the amine interaction, no other indication of product formation is visible. With CO_2 captured in MEA, however, we do not see the regeneration of the free amine (N–H bending, at 1596 cm^{-1}, SI Table S1)[41]. Instead, only some removal of MEA–CO_2 (NH_3^+, positive asymmetric bend and, (*N*–)COO^-, asymmetric stretch, visible as a shoulder at 1638 cm^{-1} and 1577 cm^{-1}, respectively)[37,40], from the surface is apparent at lower applied potentials. The band of (*N*–)COO^-, however, increased more strongly after −1.3 V vs. Ag/AgCl, in agreement with our CV results. We conclude that MEA–CO_2^- is consumed or removed from the surface, whereas MEA–H^+ is retained due to electrostatic interactions[17]. This, plus the absence of a CO_2 band at ~ 2333 cm^{-1} suggest that MEA–H^+ was blocking the surface from MEA–CO_2^- due to strong surface interactions with Cu, preventing CO_2 release and reduction (see Fig. 4H). It could also mean that the N–C bond in MEA–CO_2^- is simply too strong to break[42]. In contrast, AMP–H^+, leaves sufficient space for CO_2 reduction due to its steric hindrance (see Fig. 4I) and weaker N–C bonding[27].

Figure 4D–F shows the in situ FTIR spectra for Pb electrode in the potential range of −1.6 V to −2.5 V vs. Ag/AgCl (the complete spectra with and without CO_2 are given in Fig. S5 along with a summary of the most important bands and their changes in Tables S4 and S5). In the free CO_2 solution (Fig. 4D), we see a clear CO_2 consumption as a positive band at 2336 cm^{-1} arises (O = C = O, asymmetric stretch)[30], as well as the development of three negative bands at in the region of carboxylic acids and carboxylates (C = O and COO^- stretches at 1692, 1641 and 1607 cm^{-1})[30,39,43]. These bands intensify rapidly at −1.7 V vs. Ag/AgCl in accordance with our CV experiments, suggesting that one or more eCO_2RR products are forming[39]. Interestingly, in both MEA and AMP–CO_2 captured solution, we observe positive consumption bands of both CO_2 (2336 and 2338 cm^{-1}) and an ammonium (NH_3^+, asymmetric bend, at 1641 and 1643 cm^{-1}, respectively) and a carboxylate ((*N*–)COO^-, asymmetric stretch, at 1550 and 1560 cm^{-1}, respectively)[37,40]. This, along with a negative formation band representing the free amines (N–H bend, at 1607 and 1607 cm^{-1})[40,41] shows that the eCO_2RR occurs via the carbamate. The bands are intensified at potential around −1.9 V vs. Ag/AgCl in agreement with our CV experiments. Both instances show a band of carboxylic acid formation (C = O stretch, negative band at ~1695 cm^{-1}) that could be an eCO_2RR product, although there is also a consumption band at 1725 cm^{-1} (C = O stretch) in the same region regarding the MEA system.

Again, due to the amine interaction no other indication of product formation is visible. The similarity between the MEA and AMP solutions suggest that steric hindrance and bond strength plays less a role. Unlike for Cu electrode, CO_2 is released and immediately consumed near the surface in both amine solutions, implying that the strength of the N–C bond played no role. The outer electron transfer and the absence of a strong electrode–amine interaction at the Pb surface created a more dynamic surface system, allowing for space for CO_2 reduction and is represented in Fig. 4H–I.

Surprisingly, even though the amine regeneration clearly indicates CO_2 release, there is no CO_2 formation band. However, spontaneous CO_2 release is present in all systems (see below). This implies that eCO_2RR is mediated by the carbamate. The carbamate transfers the CO_2 molecule to the electrode, causing the eCO_2RR to occur instantaneously at the given potential[14].

Bulk electrolysis

Chronoamperometric measurements on Cu and Pb electrodes were performed at −1.8 V and −2.5 V vs. Ag/AgCl, respectively, for 2 h. The Faradaic Efficiency (FE) of liquid and gas products from CO_2 reduction reaction (free and captured) are depicted in Fig. 5 and Table 1. Average current density (mA cm^{-2}) and (released) CO_2 present in the outlet are also shown in Table 1. The FEs of possible eCO_2RR products and amount of CO_2 release every 15 min are shown in Fig. S6 and Table S6, while the FEs of blank experiments (without CO_2) are shown in Table S7 whereas the corresponding chronoamperometric measurements are shown in Fig. S7. In contrast to electrochemical CO_2 reduction in aqueous solvent on Cu electrode, where substantial amounts of C_{2+} is formed, in sulfolane solvent, Cu electrode (Fig. 5A) and free CO_2 (Table 1, entry 1) produced mainly formic acid (72%), H_2 (26%), and CO (7%)[32].

However, in the case of MEA (Table 1, entry 2), only H_2 (42%) is observed although an average of 7300 ppm of CO_2 was found in the gas outlet, indicating that CO_2 is released from MEA–CO_2.

This adds to the notion that MEA–H^+ is limiting electron transport to the desired carbamate active species and that this species is only present at the surface (represented in Fig. 5B, left)[15,23]. As a result, rather than CO_2 reduction, the proton reduction initiated by MEA–H^+ is the sole cause of the decrease in onset potential and increase in current density observed in the Fig. 3A. This indicates that MEA–H^+ is an efficient proton shuttle[24,44] that raises the local proton

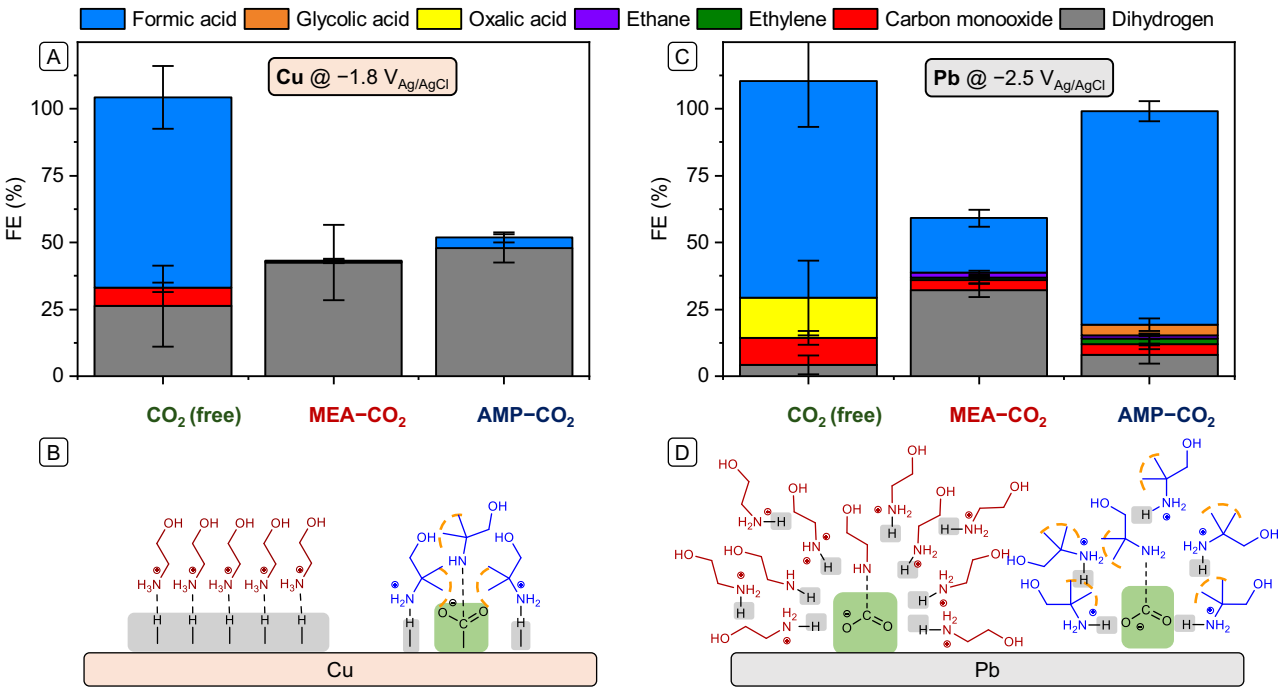

Fig. 5 | Comparison between product distribution and electrode surface. A FEs of the eCO_2RR products using a free CO_2, MEA–CO_2 and AMP–CO_2 using Cu electrode (area = 9.4 cm^2) and the **B** corresponding proposed surface interaction of the different amines with Cu surface, and **C** FEs of the eCO_2RR products using a free CO_2, MEA–CO_2 and AMP–CO_2 using Pb electrode (area = 2.76 cm^2) and **D** the corresponding proposed surface interaction with Pb of the different amines. Chronoamperometry was performed for 2 h in sat. TEACl in sulfolane at−1.8 V (Cu) or −2.5 V (Pb) vs. Ag/AgCl, respectively. *i*R compensation of 85% was applied automatically during the measurement with average resistance (*N* = 8) 8±7 Ω and 43±46 Ω for Pb and Cu, respectively. Spikes are due to sample picking by hand. Product analysis was performed by GC and HPLC. Error bars are calculated based on three individual measurements. FE Faradaic efficiency, MEA monoethanolamine, AMP 2-amino-2-methyl-1-propanol. Source data are provided as a Source Data file.

Table 1 | FEs of the eCO_2RR products, average current density (J_{avg}) and average CO_2 detected in gas outlet using a free CO_2, MEA–CO_2 and AMP–CO_2 with a Cu or a Pb WE

Entry	Amine	WE	J_{avg} (mA cm^{-2})	CO_2 in gas$_{outlet}$ (10^3, ppm)	FE (%)								
					Gaseous products						Liquid products		
					H_2	CH_4	CO	C_2H_4	C_2H_6	C_3H_6	Oxalic acid	Glycolic acid	Formic acid
1	– (CO_2)	Cu	−0.8	225	26.2 (±15.21)	–	7.0 (±1.78)	–	–	–	–	0	71.1 (±11.66)
2	MEA	Cu	−3.9	7.3	42.4 (±14.06)	–	–	0.4 (±0.58)	0.1 (±0.09)	–	–	0	0.3 (±0.76)
3	AMP	Cu	−0.5	7.5	47.8 (±5.29)	–	–	–	–	–	–	0	4.1 (±1.91)
4	– (CO_2)	Pb	−2.5	225	4.2 (±3.61)	–	10.1 (±2.53)	–	–	–	14.9 (±13.97)	0	81.0 (±17.15)
5	MEA	Pb	−5.3	7.1	32.1 (±2.46)	–	3.8 (±1.16)	1.1 (±0.51)	1.7 (±0.67)	–	–	0	20.4 (±3.10)
6	AMP	Pb	−1.3	6.9	8.1 (±15.21)	–	3.8 (±1.83)	2.2 (±1.79)	1.3 (±0.36)	–	–	3.9 (±2.31)	79.8 (±3.70)

Chronoamperometry was performed for 2 h in sat. TEACl in sulfolane at −1.8 V (Cu) or −2.5 V (Pb) vs. Ag/AgCl, respectively, and a *i*R compensation of 85% was applied. Product analysis was performed by GC and HPLC.

concentration as seen elsewhere with homogeneous eCO_2RR electrocatalysts[45].

We attribute the higher current density of 3.9 mA cm^{-2} to the proton from this species ($-NH_3^+$) being easier to reduce and more abundant than trace water in the system[23]. We see no other products, although solvent and/or amine decomposition are likely. The absence of eCO_2RR products on Cu electrode in MEA-CO_2 is supported by the in situ FTIR results (Fig. 4B), which shows no bands related to CO_2 reduction nor to carbamate consumption. When using CO_2 captured in AMP (Table 1, entry 3), a small amount of formic acid (4%) is detected next to H_2 (42%), indicating that CO_2 reduction was possible. The steric hindrance of the AMP-moiety likely enables the proximity of the AMP carbamate to the surface, facilitating the release CO_2, as depicted in Fig. 5B (right)[12].

Like with MEA, we attribute the enhancement in current density and decrease in onset potential in cyclic voltammetry (Fig. 3A) to proton reduction by AMP–H^+. However, due to the smaller likelihood of two protons being in proximity within the sterically hindered AMP, the onset potential is more negative, and the current density is lower compared to MEA. A remaining percentage of FE remains unaccounted for in both MEA and AMP systems. The surplus electrons may be involved in the breakdown reactions of solvents or amines (vide infra).

In agreement with the in situ FTIR spectra (Fig. 4), the Pb electrode shows a different product distribution during bulk electrolysis (Fig. 5C). In free CO_2 solution (Table 1, entry 3, and trace amounts of water, formic acid (81%) are identified as the main product from eCO_2RR, followed by oxalic acid (15%), CO (10%), and a minor amount of H_2 (4%)[7]. Since oxalic acid is a dimerization product of two $CO_2^{\bullet-}$ radicals, its presence indicates an outer-sphere electron transfer[31]. A considerable amount of H_2 (32%) is found in the CO_2 captured in MEA (Table 1, entry 5), indicating that MEA–H^+ is still supplying high amount of protons to the surface leading to an increase in current density (−5.3 mA cm^{-2}). Next to formic acid (20%) and CO (4%), C_2 hydrocarbons are also observed, with C_2H_6 (2%) being slightly more abundant than C_2H_4 (1%), while oxalic acid is absent. The latter showed that the initial CO_2 reduction product is stabilized by MEA, enabling additional protonation and activating the CO_2 by removing its linearity[46]. AMP (Table 1, entry 6) gives a slightly lower average current density of −1.3 mA cm^{-2}, while more formic acid (80%) is detected. Interestingly, the H_2 (8%) generation decreases considerably, and similar amounts of CO (4%) are observed. Surprisingly, glycolic acid (4%), which is one reduction step further then oxalic acid, is detected, even though oxalic acid itself is not observed. This indicates that AMP stabilizes and protonates the initial $CO_2^{\bullet-}$ less then MEA, allowing for dimerization of the radical.

C_2 hydrocarbons are also detected, albeit at very low FE (Table 1). As compared to MEA, the C_2 products generated from CO_2 captured by AMP contained fewer protons and less H_2 is produced overall, indicating that fewer protons are accessible at the surface[47]. The proton shortage is most likely caused by AMP's steric hindrance, that reduced the space available for AMP–H^+ species to approach the surface, making MEA–H^+ a better proton shuttle (see Fig. 5D).

These results contrast to previous publications on CO_2RR in aqueous solvent, where a high amount of C_{2+} hydrocarbons is produced[29,48]. The mechanism to C_2 products can either follow a C_1 pathway, where *COH is the key intermediate, leading to both methane and C_2 products, or it can follow a C_2 pathway in which C-C coupling occurs via dimerization of two adsorbed *CO[29,48,49] leading to the formation of only C_{2+} products. Our results suggest that dimerization follows the C_2 pathway because methane was not identified as a product under any of our experimental conditions (Table 1). However, the FE of C_{2+} is very low because a certain concentration of protons must be available for the hydrogenation of *CO intermediate to C_{2+} hydrocarbons. Similar results were obtained previously by our group on a Cu electrode in acetonitrile solvent in the presence of different concentrations of water. Ethylene, for instance, was detected only when the concentration of water was higher than 500 mM [32,50]. In addition, the solubility of CO, the key intermediate, is lower in organic solvent than in aqueous medium, hindering the accessibility of such species to the electrode surface.

Interestingly, the amounts of CO_2 in the gas stream are consistent across all bulk electrolysis with CO_2 captured in amines even if no products that reduce CO_2 are found. Due to the weaker R–CO_2 bond, we anticipated that AMP would release more CO_2 or that there would be a direct correlation between the current density and CO_2 release. We ran control experiments to determine whether the electrochemical experiment or the acid counter electrode compartment was responsible for the CO_2 release. The results (shown in Fig. S10) show that the CO_2 release is spontaneous.

The (positive) effect of the amines on eCO_2RR is larger on Pb than on Cu electrodes, although both amines release similar CO_2 amounts. The superiority of Cu as a hydrogen evolution electrocatalyst and the reputation of Pb as a poor proton reduction electrocatalyst are likely related[51]. A further factor is how the AMP–COO^-/–H^+ couple interacts with the surface[52].

Using Cu as an electrocatalyst might be counterproductive when using CO_2-shuttling molecules because of the good interactions with –C and –H atoms in the organic compounds[29]. Pb is less electrocatalytically active, tending to form free radicals via outer-sphere electron transfer[28,53]. If these radicals are stabilized, this electron transfer may help the CO_2 molecule react towards longer and protonated products. Another possibility is capability of the carbamates to place the CO_2 molecules near the electrode surface and removing the linearity of the CO_2 molecule. This facilitates an interaction of Pb with the oxygen atoms, causing the reaction to occur more smoothly[54]. Figure S11 illustrates a hypothesized mechanism for the influence of amines on the Cu and Pb WE.

As we expected, our findings with sulfolane solvent differ from those reported in aqueous solutions on Ag electrode[10–12,15]. While we found an amine dependence, the studies in aqueous solvents show a

weak amine dependence, although the proton shuttling effect of the formed ammonium species is clear[10,11]. The likely explanation for this difference is the prevention of bicarbonate formation, which is favored in presence of water. However, the significance of pH-dependent H-bonds through water[55] should not be overlooked.

The steric structure of amines, exemplified by the α-methyl groups in AMP, creates hindrance that affects the penetration and solvation of trace water molecules[56]. These structural differences lead to stronger hydrogen bonding of water with the AMP nitrogen atom compared to MEA. Consequently, the reactivity with CO_2 is influenced, with a temperature-dependent shift in AMP's favor that facilitates carbamate formation. Essentially, the methyl groups in AMP modulate the hydrogen bond network, impacting both solvation dynamics and interaction with CO_2 in the presence of trace water[57].

The remaining FE in Fig. 5 suggests that not all of the electrons added to the electrochemical reduction of amine–CO_2 resulted into identifiable products, particularly with MEA as the CO_2 captor on Cu electrodes, in which electrolysis of pure sulfolane and sulfolane-amine (in the absence of CO_2) showed a small current density (Fig. S7), suggesting a reduction or degradation of the solvent is taking place (Table S7 and Fig. S7), though no product was detected by either GC and HPLC (Table S7 and Figs. S8 and S9). However, in situ FTIR analysis of the pure solvent and solvent amine for both Cu and Pb electrodes characteristic bands at 3250–2750 cm^{-1}, assigned to C–H stretching of butane[58], or tetrahydrothiophene[59] which corresponds to sulfolane decomposition (cf. Figs. S4 and S5)[60,61]. This suggests that solvent degradation, particularly prevalent on copper-based systems (Fig. S4), is responsible for the FE losses observed in Fig. 5. In Figs. S7–S9, we discuss the possible reactions which may take place involving solvent degradation. In addition, we performed ^{1}H and ^{13}C nuclear magnetic resonance (NMR) spectroscopy. Our results depicted in Fig. S16 suggest that solvent decomposition indeed plays a role in the reduced FE observed in the absence of CO_2 (Fig. 5). The presence of CO_2 shifts the system toward CO_2 reduction products like formic acid, thereby improving the FE. However, the overlapping NMR signals preclude the identification of all degradation products (Fig. S17).

In summary, this study addresses the role of amines in conjunction with the cathode material in the direct electrocatalytic CO_2RR for carbon capture and utilization. Our results contribute to understanding the role and mechanism of amines in direct electrocatalytic CO_2 reduction in carbon capture and utilization. Amines play an active part in surface mechanisms. We show that various factors influence this process, such as steric hindrance, carbamate bond strength, induced local proton concentration, and electrocatalytic electron transfer. Cu (inner-sphere electron transfer) and Pb (outer-sphere electron transfer) were compared as CO_2 reduction electrocatalysts. Two model amines, MEA (no steric hindrance, strong CO_2 bond) and AMP (steric hindrance, weak CO_2 bond) were used to study the effects of amines. We demonstrate that the ammonium species created during the CO_2 collection step dominate the free CO_2 reduction process on Cu electrodes. MEA–CO_2 reduces more readily than AMP–CO_2, indicating that one of the two species in the MEA–CO_2 couple, ($R–COO^-/–H^+$), has a stronger affinity for the Cu surface. FTIR experiments confirm that the AMP–CO_2 is converted to free AMP and that CO_2 reduction occurs, which is absent in the case of MEA. We theorize that MEA–H^+ prevents interaction with the Cu surface with released CO_2, whereas AMP–H^+ permits some CO_2 reduction due to steric hindrance, which enables the CO_2 to reach the surface. As a result, rather than CO_2 reduction, the proton reduction initiated by the ammonium species is the sole cause of the decrease in onset potential and increase in current density observed in the CV. This is supported by bulk electrolysis on Cu electrodes showing that MEA–CO_2 only produces H_2 as the reduction product, whereas AMP–CO_2 also produces small amounts of acid to complement our FTIR results. This suggests that employing inner-sphere electrodes—such as Cu—while utilizing CO_2-shuttling compounds may not be beneficial since these cathodes enhance interaction with organic molecules because of their strong bonds with atoms of the –C and –H.

Conversely, when Pb electrodes are used, the free eCO_2RR is more active than amines–CO_2 adducts. Compared to Cu, the applied potential difference between MEA–CO_2 and AMP–CO_2 where the current density is accelerated, is significantly less. The conversion of MEA–CO_2 and AMP–CO_2 to free MEA and AMP as well as the reduction of CO_2 are both confirmed in both cases by FTIR. By showing that the variation in steric hindrance and C–N bond strength of the carbamates has less of an effect on the Pb electrode, we conclude that there are fewer surface interactions, resulting in a more dynamic surface environment. This supports our hypotheses that outer-sphere electrodes, such as Pb, are more suitable for direct carbamate reduction and that substrate absorption on the surface is not beneficial. Indeed, bulk electrolysis on Pb showed eCO_2RR products when MEA–CO_2 and AMP–CO_2 are used as a CO_2 donor. Interestingly, the amines–CO_2 adducts yield more protonated products. The presence of extra protons from ammonium species in bulk electrolysis promotes the production of protonated eCO_2RR products. Comparing MEA and AMP, we see that MEA–H^+ has superior proton shuttling capabilities, resulting in higher proton content in C_2 products. This implies that MEA–H^+ is less hampered by steric hindrance.

The amount of CO_2 in the gas stream remained consistent across all bulk electrolysis with CO_2 captured in amines, even though no CO_2 reduction products were discovered. Surprisingly, no CO_2 forming band is visible in FTIR even though the amine regeneration clearly indicates CO_2 release. We hypothesize that the carbamate functions as a mediator, causing the CO_2 molecule to be activated and transferred to the electrode, making the eCO_2RR instant at the specified potential. Overall, our results open new opportunities for designing combined electrochemical/chemical absorption setups for effective carbon capture and utilization. Unraveling the complex mechanisms of amine-based CO_2 reduction could encourage the development of template amines that dictate the product composition in CO_2 reduction outcomes.

Methods

Additional details on the experiments performed in this study are found in the SI.

Chemicals and electrodes

All reagents and solvents were used without purification unless noted otherwise. Fresh solutions were prepared for each experiment, and all electrochemical reactions were performed under atmospheric condition and at room temperature unless otherwise noted. All water was purified using a Milli-Q Millipore system (Merck Milli-Q IQ 7000 Ultrapure Lab Water System, Millipak 0.22-μm Filter) with a total organic carbon content <3 ppb and a resistivity higher than 18 MΩ·cm at room temperature. All glassware was previously cleaned using a standard acidic permanganate cleaning procedure. All glassware and tools, including three-electrode glass cells and PEEK bulk electrolysis cells, were soaked in a solution of 1 g L^{-1} $KMnO_4$ and 0.5 M H_2SO_4 in Milli-Q water. After decanting the excess solution for reuse, the glassware was rinsed three times with Milli-Q water, then soaked for at least 30 min in a freshly prepared piranha solution (approximately 10 mL H_2SO_4 and 3 mL H_2O_2 per liter of Milli-Q). This step oxidized organic materials and reduced MnO_2 and residual MnO_4^-. The glassware was then rinsed three times with Milli-Q water and boiled three times to remove the remaining ions. Finally, the glassware was stored submerged in Milli-Q water and further dried at 130 °C before use (for more details, see details in the SI, Section S3).

During measurement, solutions were purged with nitrogen gas (N_2, 99.999%, Linde) or carbon dioxide gas (CO_2, 99.5%, Linde).

The amines used in this study are monoethanolamine (MEA, >99.0%, TCI Europe N.V.) and 2-amino-2-methyl-1-propanol (AMP, >93.0% TCI Europe N.V) and a standard electrolyte of a saturated solution of tetraethylammonium chloride (≥98.0%, TEACl, VWR International B.V.) in tetrahydrothiophene 1,1-dioxide (sulfolane, ≥99.0%, Sigma-Aldrich) was used. The average water content of the electrolyte was >1000 ppm, determined by measuring 0.2 mL on a Metrohm 831 Karl-Fischer Coulometer. The following chemicals were used in cleaning and polishing: $KMnO_4$ (VWR International B.V., GPR RECTAPUR), H_2SO_4 (95–98%, Sigma-Aldrich), H_2O_2 (30%, Sigma-Aldrich), and H_3PO_4 (85%, VWR International B.V.). The following electrodes were used for CV and in situ FTIR experiments: a Pb disk (99.99 + %, MaTecK, Ø = 5 mm, $A_{geo} = 0.196\ cm^2$) or a Cu disk (99.99 + %, MaTecK, Ø = 5 mm, $A_{geo} = 0.196\ cm^2$) working electrodes (WE), a Pt wire (0.5 mm, 99.9 %, MatecK) counter electrode (CE) and a Ag/AgCl reference electrode (RE, 3.0 M KCl leakless Ag/AgCl,). For bulk electrolysis, the following electrodes were used: Pb wire (Advent, 99.999%, Ø = 2 mm of $A_{geo} = 2.76\ cm^2$) or Cu wire (99.99 + %, MaTecK, Ø = 1 mm, $A_{geo} = 9.40\ cm^2$) as WE, a Pt mesh CE (2.0 cm × 2.0 cm, 0.1 mm wire diameter, 99.9%, Sigma-Aldrich) and Ag/AgCl RE (3.0 M KCl miniature leakless Ag/AgCl).

The Pb and Cu WE used in this study were treated by (electro-) polishing before each measurement. The Pb WE was mechanically polished using a diamond polishing paste (Buehler, MetaDiTM, 1 μm) on a small rectangular felt polishing pad (MicroCloth, PSA backing, Buehler) following a figure-8 hand movement, or it was polished with a Kleenex wipe until shiny. After that, the Pb electrode was electropolished in an aqueous 0.5 M H_2SO_4 solution using Pt as the RE and CE at −2.5 V vs. Pt for 500 s[4]. Prior to usage, the Cu electrode was electropolished using another Cu as the RE and CE in an aqueous solution of 66% (v/v%) H_3PO_4 for 3 × 10 s at 3.0 V vs. Cu. The Pt CE was flame annealed, and the Ag/AgCl RE was washed with the electrolyte solution before use. The calibration of Ag/AgCl was done by measuring the ferrocene/ferrocenium$^+$ redox couple in the sat. TEACl in sulfolane electrolyte. CV measurements were performed using a three-electrode configuration at ambient temperature with a glassy carbon (GC) (Tarek Equilabrium, Ø = 6 mm, $A_{geo} = 0.28274\ cm^2$) WE, a flame annealed Pt CE, and a normal or miniature leakless Ag/AgCl reference electrode (Ø = 5 mm ET069, eDAQ or Ø = 2 mm ET072 eDAQ, respectively). The GC WE was hand polished following a figure 8 hand movement of the WE with a diamond polishing paste (Buehler, MetaDiTM, 1 μm) on a small rectangular piece of felt polishing pad (MicroCloth, PSA backing, Buehler). The solution containing the ferrocene/ferrocenium$^+$ redox couple was magnetically stirred during degassing and between each measurement. Measurements were taken starting from 0.25 to 0.67 V vs. Ag/AgCl and back with a scan rate of 100 mV s^{-1} and three scans were taken. The obtained result is shown in Fig. S2D.

In this study, all potentials are refereed to Ag/AgCl scale, for comparison it corresponds to the 0.197 V vs. NHE.

Procedure for preparing MEA−CO_2 and AMP−CO_2

A 1.0 M amine solution in (sat. TEACl in sulfolane) was saturated with CO_2 (10 mL min^{-1}) for 15 min to fully convert the amine to the ammonium and carbamate species. The solution was then purged for 15 min with N_2 gas (10 mL min^{-1}) to remove any remaining dissolved CO_2, generating the carbamate as the only CO_2 source, after which CV was performed. Control experiments were carried out by additionally purging the solution for 15 min with N_2 gas (10 mL min^{-1}) and gave identical results, confirming the full removal of CO_2 (for details, see SI, Section S4.2 and the resulting data as shown in Figs. 2B, C and S12A, B).

Procedure for cyclic voltammetry experiments

Cyclic voltammetry (CV) measurements were performed using a three-electrode configuration in an undivided four-necked heart-shaped cell (Fig. S1A) at ambient temperature and pressure, filled with 5 mL of solution. Pb disk or Cu disk were used as WE, and Pt wire and Ag/AgCl as CE and RE, respectively. The WE, CE, and RE were prepared as previously explained. All CVs were recorded with a Metrohm Multi Autolab potentiostat (M204, serial number MAC90609) controlled by Nova 2.1 software. The obtained data is exported as txt file and later processed using either Excel or origin software. The resistance of the solution was determined prior to each measurement using the *i*-interrupt program and the potential was corrected for the *i*R drop by applying a correction of 85% of the solution resistance. The iR compensation was automatically applied by the potentiostat with average resistance ($N = 8$) 667±263 Ω and 530±197 Ω for Pb and Cu, respectively. Figures without *i*R compensation are shown in Fig. S18. The standard electrolyte consisted of a saturated solution of TEACl in sulfolane (5 mL). Freshly prepared solutions were magnetically stirred during (de-)gassing and between each measurement. Measurements were taken from the more positive to the more negative potential and back with −1.0 V to −2.5 V vs. Ag/AgCl (Pb) or with −1.0 V to −1.8 V vs. Ag/AgCl (Cu) with a scan rate of 10 mV s^{-1} and three scans were taken (for details on the experimental setup see SI, section S4).

Electrochemical in situ Fourier transform infrared spectroscopy

In situ Fourier-Transform infrared (FTIR) spectroscopy was performed to study possible intermediates and products during the electrochemical experiment. The spectra were measured on a Bruker Vertex 80-V IR spectrometer equipped with a liquid nitrogen-cooled MCT detector. A Veemax III (PIKE Technologies) was positioned in the spectrometer, wherein a homemade three-electrode spectro-electrochemical cell (Fig. S1B) with a CaF_2 prism attached to the bottom was placed[62]. The cell was filled with the electrolyte with(-out) amine (~20 mL). Either Cu or Pb disk electrodes were used as the WE, whereas a Pt wire and Ag/AgCl were used as counter and reference electrodes, respectively (for electrode preparation details, see SI, section S2). The WE was pressed against the CaF_2 prism to obtain a thin film configuration[62]. The thin film was refreshed after a full experimental set. FTIR spectra were collected in a range of 4000–900 cm^{-1} at a resolution of 8 cm^{-1} with averaging 128 scans. We removed data from the range 1250–900 cm^{-1} due to the interference of strong solvent bands. All chronoamperometry experiments were performed with a Metrohm Autolab potentiostat controlled by Nova 2.1 software. The obtained data is exported as txt file and later processed using either excel or origin software. Spectra were collected over a potential range in 0.1 V decrements from −1.0 V to −1.8 V vs. Ag/AgCl (Cu) or from −1.6 V to −2.5 V vs. Ag/AgCl (Pb). The applied potential was not compensated for *i*R drop. A baseline was subtracted using the spectra obtained at −1.0 V (Cu) or −1.6 V (Pb) vs. Ag/AgCl. Spectra are presented as reflectance, according to $A = -\log(R/R_0)$, where R and R_0 are the correspond to the single beam spectra obtained at the sample and reference potentials, respectively. Positive bands (pointing up) in reflectance spectra correspond to species that were present on or near the electrode surface at the reference potential and are "consumed or removed from the surface" at the sample potential. Negative bands (pointing down) represent the "formation or accumulation of products or species on the surface" at the sample potential (for details about the cell, see SI, section S5).

Electrochemical bulk electrolysis

Bulk electrolysis was performed in a PEEK two-compartment (divided) cell designed for online gas chromatography (GC) analysis during the experiment (the cell design is shown in Fig. S1C). The cell was operated by an IVIUM Vertex.s potentiostat/galvanostat controlled by IviumSoft 4.1113 software. The obtained data is exported as txt file and later processed using either excel or origin software. The potential was corrected for the *iR* drop by applying a correction of 85% of the resistance, determined at the start of the experiment by Electrochemical Impedance Spectroscopy (EIS), the default setting in

IviumSoft and is automatically applied by the potentiostat. iR Average resistance ($N = 8$) 8±7 Ω and 43±46 Ω for Pb and Cu, respectively. The anodic (counter electrode compartment, CEC) and cathodic (working electrode compartment, WEC) compartments were separated by a pretreated Nafion−117 membrane (thickness = 170 microns, 5 × 5 cm) that was patted dry with tissue paper and then placed between the two compartments. Before its use, Nafion−117 membranes were cleaned by heating in Milli-Q water at 80 °C for 60 min, followed by three cycles in 3 wt% H_2O_2 solution, and then in 1.0 M H_2SO_4 solution, each heated to 80 °C for 60 min and rinsed with Milli-Q water. This process was repeated three times, and the membranes were stored in fresh Milli-Q water until needed[63,64]. The WEC was made up of a Cu or Pb WE and a miniature leakless Ag/AgCl RE immersed in a sat. TEACl in sulfolane solution (8 mL) with or without 1.0 M amine. The CEC held a Pt mesh CE in a 0.5 M H_2SO_4 aqueous solution (8 mL). A gas flow of either N_2 or CO_2 was controlled by a Brooks Mass Flow Controller (Model O254). For CO_2 electroreduction with gaseous products, the CO_2 flow rate was measured using the same mass flow controller to maintain a consistent flow rate of 5 mL/min throughout the experiment, ensuring accurate and controlled delivery of CO_2 to the electrochemical cell. Gas samples were analyzed every 5 min by gas chromatography (Agilent 990 Micro GC). Samples were taken from 15 min before the start and until the end of the electrolysis. Chronoamperometric experiments were performed for 2-h at −2.5 V and −1.8 V vs. Ag/AgCl for the Pb and Cu WE, respectively. The bulk electrolysis method is further discussed in SI, Section S6.

Qualitative and quantitative liquid and gas product analysis were done with high-performance liquid chromatography (HPLC) and gas chromatography (GC).

For the GC analysis, it was used a gas chromatograph (Agilent 990 Micro GC) with two thermal conductivity detectors (TCD). Gas samples were automatically taken every 5 min and analyzed on a Molsieve column (MS5A SS 10 m × 0.25 mm × 30 μm, Agilent) for H_2, O_2, N_2, CH_4, CO, and on a CP-PoraPLOT U column (10 m × 0.25 mm × 8 μm, Agilent) for CO_2, ethene, ethane, propene, and H_2O. Molsieve column parameters: Ar carrier gas, 110 °C injection temperature, 50 ms injection time, 14 s backflush, 80 °C column temperature, 200 kPa initial pressure, 120-second run time. PoraPLOT column parameters: He carrier gas, 110 °C injection temperature, 50 ms injection time, no backflush, 80 °C column temperature, 200 kPa initial pressure, 120-second run time. Calibration curves for all gases, using Nippon calibration gas with specific concentrations, are shown in Fig. S12. The Faradaic efficiency for every measured time was calculated according to Equation S1.

HPLC analyses were carried out in high-performance liquid chromatography (HPLC, Agilent 1260, Infinity II). Samples (50 μL) were diluted with 1000 μL of Milli-Q water and analyzed on an ion exclusion column (Bio-Rad Aminex HPX-87H) for small, polar products from CO_2 reduction (formic acid, glycolic acid, oxalic acid). The column was coupled with a variable wavelength detector (VWD, G7114A) and a refractive index detector (RID, G7162A). Analysis was performed at 50 °C with a 5 mM H_2SO_4 aqueous mobile phase, a flow rate of 0.5 mL min^{-1}, an injection volume of 20 μL, and a 35-min cycle. Product concentrations were determined by normalizing the product peak area to the peak of sulfolane (internal standard) and applying a conversion factor from calibration curves (Fig. S13). The Faradaic efficiency was calculated according to Equation S4. (For more details on the HPLC and GC procedure, see SI, section S7–8).

Data availability

The Data Source generated in this study have been deposited in the Figshare database (https://doi.org/10.6084/m9.figshare.27037306). The processed data are available at Figshare. The data generated in this study are provided in the Supplementary Information/Source Data file (https://figshare.com/s/5ee9d0a8ae1f301f29c8). Source data are provided with this paper.

References

1. Al-Mamoori, A., Krishnamurthy, A., Rownaghi, A. A. & Rezaei, F. Carbon capture and utilization update. *Energy Technol.* **5**, 834–849 (2017).
2. Gregory, L. B. & Scharmann, W. G. Carbon dioxide scrubbing by amine solutions. *Ind. Eng. Chem.* **29**, 514–519 (1937).
3. Meng, F. et al. Research progress of aqueous amine solution for CO_2 capture: a review. *Renew. Sustain. Energy Rev.* **168**, 112902 (2022).
4. Rochelle, G. T. Amine scrubbing for CO $_2$ capture. *Science* **325**, 1652–1654 (2009).
5. Said, R. Ben, Kolle, J. M., Essalah, K., Tangour, B. & Sayari, A. A unified approach to CO $_2$ –amine reaction mechanisms. *ACS Omega* **5**, 26125–26133 (2020).
6. Yamada, H. Amine-based capture of CO_2 for utilization and storage. *Polym. J.* **53**, 93–102 (2021).
7. Pérez-Gallent, E., Vankani, C., Sánchez-Martínez, C., Anastasopol, A. & Goetheer, E. Integrating CO_2 capture with electrochemical conversion using amine-based capture solvents as electrolytes. *Ind. Eng. Chem. Res* **60**, 4269–4278 (2021).
8. Liu, G. et al. Integrated CO_2 capture and utilisation: a promising step contributing to carbon neutrality. *Carbon Capture Sci. Technol.* **7**, 100116 (2023).
9. Li, M., Irtem, E., Iglesias van Montfort, H.-P. P., Abdinejad, M. & Burdyny, T. Energy comparison of sequential and integrated CO_2 capture and electrochemical conversion. *Nat. Commun.* **13**, 5398 (2022).
10. Shen, K. et al. On the origin of carbon sources in the electrochemical upgrade of CO_2 from carbon capture solutions. *Joule* **7**, 1260–1276 (2023).
11. Leverick, G. et al. Uncovering the active species in amine-mediated CO_2 reduction to CO on Ag. *ACS Catal.* **13**, 12322–12337 (2023).
12. Jerng, S. E. & Gallant, B. M. Electrochemical reduction of CO_2 in the captured state using aqueous or nonaqueous amines. *iScience* **25**, 104558 (2022).
13. Chen, L. et al. Electrochemical reduction of carbon dioxide in a monoethanolamine capture medium. *ChemSusChem* **10**, 4109–4118 (2017).
14. Abdinejad, M., Mirza, Z., Zhang, X. & Kraatz, H.-B. Enhanced electrocatalytic activity of primary amines for CO_2 reduction using copper electrodes in aqueous solution. *ACS Sustain Chem. Eng.* **8**, 1715–1720 (2020).
15. Lee, G. et al. Electrochemical upgrade of CO_2 from amine capture solution. *Nat. Energy* **6**, 46–53 (2020).
16. Bhattacharya, M., Sebghati, S., Vercella, Y. M. & Saouma, C. T. Electrochemical reduction of carbamates and carbamic acids: implications for combined carbon capture and electrochemical CO_2 recycling. *J. Electrochem Soc.* **167**, 086507 (2020).
17. Khurram, A., Yan, L., Yin, Y., Zhao, L. & Gallant, B. M. Promoting amine-activated electrochemical CO_2 conversion with alkali salts. *J. Phys. Chem. C.* **123**, 18222–18231 (2019).
18. Sullivan, I. et al. Coupling electrochemical CO_2 conversion with CO_2 capture. *Nat. Catal.* **4**, 952–958 (2021).
19. Siegel, R. E., Pattanayak, S. & Berben, L. A. Reactive capture of CO_2: opportunities and challenges. *ACS Catal.* **13**, 766–784 (2023).
20. Kar, S., Goeppert, A. & Prakash, G. K. S. Integrated CO_2 capture and conversion to formate and methanol: connecting two threads. *Acc. Chem. Res* **52**, 2892–2903 (2019).
21. Massen-Hane, M., Diederichsen, K. M. & Hatton, T. A. Engineering redox-active electrochemically mediated carbon dioxide capture systems. *Nat. Chem. Eng.* **1**, 35–44 (2024).

22. Xia, Q. et al. Integration of CO_2 capture and electrochemical conversion. *ACS Energy Lett.* **8**, 2840–2857 (2023).
23. Safipour, J., Weber, A. Z. & Bell, A. T. Detrimental effects of monoethanolamine and other amine-based capture agents on the electrochemical reduction of CO_2. *ACS Energy Lett.* **8**, 5012–5017 (2023).
24. Yang, L. et al. Promoting CO_2 electroreduction to acetate by an amine-terminal, dendrimer-functionalized Cu catalyst. *ACS Cent. Sci.* **9**, 1905–1912 (2023).
25. Muchan, P. et al. Effect of number of hydroxyl group in sterically hindered alkanolamine on CO_2 capture activity. *Energy Procedia* **114**, 1966–1972 (2017).
26. Yin, L., Li, X., Zhang, L. & Li, J. Characteristics of carbon dioxide desorption from MEA-based organic solvent absorbents. *Int. J. Greenh. Gas. Control* **104**, 103224 (2021).
27. Yoon, B., Calabro, D. C., Baugh, L. S., Raman, S. & Hwang, G. S. Probing strong steric hindrance effects in aqueous alkanolamines for CO_2 capture from first principles. *J. Environ. Chem. Eng.* **10**, 108987 (2022).
28. Boettcher, S. W. & Surendranath, Y. Heterogeneous electrocatalysis goes chemical. *Nat. Catal.* **4**, 4–5 (2021).
29. Nitopi, S. et al. Progress and perspectives of electrochemical CO_2 reduction on copper in aqueous electrolyte. *Chem. Rev.* **119**, 7610–7672 (2019).
30. Figueiredo, M. C., Ledezma-Yanez, I. & Koper, M. T. M. In situ spectroscopic study of CO_2 electroreduction at copper electrodes in acetonitrile. *ACS Catal.* **6**, 2382–2392 (2016).
31. Eneau-Innocent, B., Pasquier, D., Ropital, F., Léger, J. M. & Kokoh, K. B. Electroreduction of carbon dioxide at a lead electrode in propylene carbonate: a spectroscopic study. *Appl Catal. B* **98**, 65–71 (2010).
32. Deacon-Price, C., da Silva, A. H. M., Santana, C. S., Koper, M. T. M. & Garcia, A. C. Solvent effect on electrochemical CO_2 reduction reaction on nanostructured copper electrodes. *J. Phys. Chem. C.* **127**, 14518–14527 (2023).
33. Yang, Z., Oropeza, F. E. & Zhang, K. H. L. P-block metal-based (Sn, In, Bi, Pb) electrocatalysts for selective reduction of CO_2 to formate. *APL Mater.* **8**, 060901 (2020).
34. Lv, W., Zhang, R., Gao, P., Gong, C. & Lei, L. Electrochemical reduction of carbon dioxide with lead cathode and zinc anode in dry acetonitrile solution. *J. Solid State Electrochem.* **17**, 2789–2794 (2013).
35. Trasatti, S. Work function, electronegativity, and electrochemical behaviour of metals. *J. Electroanal. Chem. Interfacial Electrochem.* **33**, 351–378 (1971).
36. Christensen, P. A., Hamnett, A., Muir, A. V. G. & Freeman, N. A. CO_2 reduction at platinum, gold and glassy carbon electrodes in acetonitrile. *J. Electroanal. Chem. Interfacial Electrochem.* **288**, 197–215 (1990).
37. Richner, G. & Puxty, G. Assessing the chemical speciation during CO_2 absorption by aqueous amines using in situ FTIR. *Ind. Eng. Chem. Res.* **51**, 14317–14324 (2012).
38. Taccone, M. I. et al. Infrared action spectroscopy of the deprotonated formic acid trimer, trapped in helium nanodroplets. *Phys. Chem. Chem. Phys.* **25**, 10907–10916 (2023).
39. Gomes, J. F. et al. Influence of silver on the glycerol electrooxidation over AuAg/C catalysts in alkaline medium: a cyclic voltammetry and in situ FTIR spectroscopy study. *Electrochim. Acta* **144**, 361–368 (2014).
40. Zanone, A., Tavares, D. T. &de Paiva, J. L. An FTIR spectroscopic study and quantification of 2-amino-2-methyl-1-propanol, piperazine and absorbed carbon dioxide in concentrated aqueous solutions.*Vib. Spectrosc.* **99**, 156–161 (2018).
41. Sun, C. & Dutta, P. K. Infrared spectroscopic study of reaction of carbon dioxide with aqueous monoethanolamine solutions. *Ind. Eng. Chem. Res.* **55**, 6276–6283 (2016).
42. Buvik, V., Vevelstad, S. J., Brakstad, O. G. & Knuutila, H. K. Stability of structurally varied aqueous amines for CO_2 capture. *Ind. Eng. Chem. Res.* **60**, 5627–5638 (2021).
43. Zhu, S., Li, T., Cai, W.-B. & Shao, M. CO_2 electrochemical reduction as probed through infrared spectroscopy. *ACS Energy Lett.* **4**, 682–689 (2019).
44. Coskun, O. K. et al. Tailoring electrochemical CO_2 reduction on copper by reactive ionic liquid and native hydrogen bond donors. *Angew. Chem. Int. Ed.* https://doi.org/10.1002/anie.202312163 (2023).
45. Jakobsen, J. B., Rønne, M. H., Daasbjerg, K. & Skrydstrup, T. Are amines the holy grail for facilitating CO_2 reduction? *Angew. Chem. Int. Ed.* **60**, 9174–9179 (2021).
46. Gao, G. et al. New insights into the structure-activity relationship for CO_2 capture by tertiary amines from the experimental and quantum chemical calculation perspectives. *Chem. Eng. J.* **473**, 145277 (2023).
47. Savéant, J. Proton relays in molecular catalysis of electrochemical reactions: origin and limitations of the boosting effect. *Angew. Chem. Int. Ed.* **58**, 2125–2128 (2019).
48. Kortlever, R., Shen, J., Schouten, K. J. P., Calle-Vallejo, F. & Koper, M. T. M. Catalysts and reaction pathways for the electrochemical reduction of carbon dioxide. *J. Phys. Chem. Lett.* **6**, 4073–4082 (2015).
49. Calle-Vallejo, F. & Koper, M. T. M. Theoretical considerations on the electroreduction of CO to C_2 species on Cu(100) electrodes. *Angew. Chem. Int. Ed.* **52**, 7282–7285 (2013).
50. Todorova, T. K., Schreiber, M. W. & Fontecave, M. Mechanistic understanding of CO_2 reduction reaction (CO2RR) toward multicarbon products by heterogeneous copper-based catalysts. *ACS Catal.* **10**, 1754–1768 (2020).
51. Gütz, C. et al. Leaded bronze: an innovative lead substitute for cathodic electrosynthesis. *ChemElectroChem* **5**, 247–252 (2018).
52. Nam, D. H. et al. Molecular enhancement of heterogeneous CO_2 reduction. *Nat. Mater.* **19**, 266–276 (2020).
53. Ali, T. et al. Electro-synthesis of organic compounds with heterogeneous catalysis. *Adv. Sci.* **10**, 2205077 (2023).
54. Lei, Y. et al. Recent advances on electrocatalytic CO_2 reduction to resources: target products, reaction pathways and typical catalysts. *Chem. Eng. J.* **453**, 139663 (2023).
55. Bagger, A., Arnarson, L., Hansen, M. H., Spohr, E. & Rossmeisl, J. Electrochemical CO reduction: a property of the electrochemical interface. *J. Am. Chem. Soc.* **141**, 1506–1514 (2019).
56. Martins-Costa, M. T. C. & Ruiz-López, M. F. Reactivity of monoethanolamine at the air–water interface and implications for CO_2 capture. *J. Phys. Chem. B* **128**, 1289–1297 (2024).
57. Snuffin, L. L., Whaley, L. W. & Yu, L. Catalytic electrochemical reduction of CO_2 in ionic liquid EMIMBF3Cl. *J. Electrochem Soc.* **158**, F155 (2011).
58. Pele, L., Šebek, J., Potma, E. O. & Benny Gerber, R. Raman and IR spectra of butane: anharmonic calculations and interpretation of room temperature spectra. *Chem. Phys. Lett.* **515**, 7–12 (2011).
59. Bezverkhyy, I., Bouguessa, K., Geantet, C. & Vrinat, M. Adsorption of tetrahydrothiophene on faujasite type zeolites: breakthrough curves and FTIR spectroscopy study. *Appl Catal. B* **62**, 299–305 (2006).
60. Ugata, Y. et al. Understanding the reductive decomposition of highly concentrated Li salt/sulfolane electrolytes during Li deposition and dissolution. *ACS Appl. Energy Mater.* **4**, 1851–1859 (2021).
61. Yu, L., Khan, M. F. & Achari, G. A review on physiochemical treatment of sulfolane in aqueous media. *J. Environ. Chem. Eng.* **9**, 105691 (2021).

62. García, G., Rodríguez, P., Rosca, V. & Koper, M. T. M. Fourier transform infrared spectroscopy study of CO electro-oxidation on Pt(111) in alkaline media. *Langmuir* **25**, 13661–13666 (2009).
63. Jiang, B. et al. Insights into the impact of the nafion membrane pretreatment process on vanadium flow battery performance. *ACS Appl. Mater. Interfaces* **8**, 12228–12238 (2016).
64. Kuwertz, R., Kirstein, C., Turek, T. & Kunz, U. Influence of acid pretreatment on ionic conductivity of Nafion® membranes. *J. Memb. Sci.* **500**, 225–235 (2016).

Acknowledgements

D.F.B. and A.C.G. gratefully acknowledge the Dutch Research Council (NWO) for providing financial support for project number ECCM.TT.MVITU.005 which are carried out in the framework of the Electrochemical Conversion and Materials (ECCM) program.

Author contributions

D.F.B. contributed to all experimental works, data analysis, manuscript preparation and conceived of the presented idea. G.R. contributed to manuscript preparation. A.C.G. contributed to FTIR measurements, manuscript preparation, conceived the project and supervision and discussion of the project.

Competing interests

The authors declare no competing interests.

Additional information

Supplementary information The online version contains supplementary material available at https://doi.org/10.1038/s41467-024-53543-4.

Correspondence and requests for materials should be addressed to A. C. Garcia.

Peer review information *Nature Communications* thanks Meng Lin, and the other, anonymous, reviewer(s) for their contribution to the peer review of this work. A peer review file is available.